Proceedings of the 9th U.S. National and 10th Canadian Conference on Earthquake Engineering
Compte Rendu de la 9ième Conférence Nationale Américaine et
10ième Conférence Canadienne de Génie Parasismique
July 25-29, 2010, Toronto, Ontario, Canada • Paper No 1315

TOWARDS QUANTIFYING MOVEMENT OF A MASSIVE LATERAL SPREAD USING HIGH-RESOLUTION SATELLITE IMAGE PROCESSING

B.R. Cox[1], J. Cothren[2], A. Barnes[3], J. Wartman[4], A. Rodriguez-Marek[5], J. Meneses[6]

ABSTRACT

During the August 15, 2007 Pisco, Peru Earthquake (Mw=8.0), a massive liquefaction-induced lateral spread occurred in Holocene marine deposits near Canchamaná, Peru. Immediately after the earthquake several of the author's documented this lateral spread in the field as part of a Geo-Engineering Extreme Events Reconnaissance (GEER) mission, and estimated it to be at least 3-km long by 1-km wide. At approximately the midpoint of this feature, the cumulative lateral displacement (obtained from adding up the widths of tension cracks) totaled more than 5 m. However, due to the large size of the feature, it was difficult to spatially quantify the magnitude of the displacements in the field, firmly establish its boundaries, and discern if the entire area moved as a coherent lateral spread toward the ocean. Therefore, pre- and post-earthquake high-resolution satellite images of the area were acquired and analyzed as a means to determine the magnitude and spatial variability of the lateral displacements. Due to a limited budget, the satellite images could not be purchased as desired for optimum processing. Despite this limitation, results from preliminary analyses are promising, confirming significant lateral movement (up to 5 m) in the marine deposits. However, due to limitations in the initial satellite images and supporting data (ground truth, digital elevation models, etc.) the absolute magnitude and vector directions of the displacements obtained from the preliminary analyses are suspected not to be fully accurate. Therefore, higher quality images are currently being purchased and processed to determine if the preliminary results can be improved upon. The tasks of the current research are to determine: (1) if high-resolution satellite image processing can be used to quantify the extent, magnitude, and direction of displacements associated with lateral spreading, and (2) what quality of raw satellite images and level of processing (i.e. cost) is needed to achieve accurate results. This paper details steps that have been taken toward answering these questions.

[1]Assistant Professor, Dept. of Civil Engineering, University of Arkansas, 4190 Bell Engineering Center, Fayetteville, AR 72701, USA, brcox@uark.edu
[2]Associate Professor, Dept. of Geosciences, Center for Advanced Spatial Technologies, University of Arkansas, JBHT 304, Fayetteville, AR 72701, USA, jcothren@cast.uark.edu
[3]Research Assistant, Dept. of Geosciences, Center for Advanced Spatial Technologies, University of Arkansas, JBHT 304, Fayetteville, AR 72701, USA, abarnes@cast.uark.edu
[4]Associate Professor, Dept. of Civil, Architectural, and Environmental Engineering, Drexel University, 2141 Chestnut Street, Philadelphia, PA 19104, USA, joe.wartman@drexel.edu
[5]Associate Professor, Dept. of Civil and Environmental Engineering, Washington State University, PO Box 642910, Pullman, WA 99164, USA, adrian@wsu.edu
[6]Chair, Seismic and GeoHazards Group, Kleinfelder, 5015 Shoreham Place, San Diego, CA 92122, USA, JMeneses@kleinfelder.com

Introduction

The M_w8.0 Pisco, Peru Earthquake of 15 August 2007 struck the coastal and inland mountainous regions of central Peru (epicenter approximately 150 km south of Lima), causing severe damage to the cities of Pisco, Ica, Cañete, Chincha, and Tambo de Mora, killing more than 500 people (INDECI 2007). The earthquake was a result of the subduction process between the Nazca plate and the South American continental plate, and was recorded at 16 strong motion stations within 150 km of the fault. All of the Pisco Earthquake records show two distinct phases of strong ground motion with long durations of shaking (~ 100 seconds) (Rodriguez-Marek et al. 2007). The two closest stations were located on 'soil' sites in Ica, approximately 38 km above the fault rupture plane. One recorded a peak ground acceleration (PGA) of 0.5 g and the other recorded a PGA of 0.34 g.

Immediately following the event, the U.S. National Science Foundation (NSF)-supported Geo-Engineering Extreme Events Reconnaissance (GEER) organization deployed a reconnaissance team to document the geotechnical aspects of the earthquake. This was a limited budget, short-term mission intended to be a perishable data gathering effort. From a geotechnical perspective, the GEER team determined that the Pisco Earthquake was most significant in terms of the amount of soil liquefaction, the number of landslides, and the marked levels of damage to urban areas and infrastructure systems (transportation and lifelines) caused by these two phenomena (Rodriguez-Marek et al. 2007). Notable liquefaction case histories documented on the mission included a massive lateral spread at least 3-km long by 1-km wide (the topic of the current paper), a 400-m long slope failure induced by liquefaction at its toe (potentially linked to the massive lateral spread), and spectacular one- to two-story building foundation failures resulting in up to 0.90 m of settlement (near the southern boundary of the massive lateral spread). All of these liquefaction failures were found in close proximity to the coast. This paper describes a massive liquefaction-induced lateral spread, and discusses the application of satellite remote sensing to quantify and better understand the mechanisms governing this extraordinary feature.

The Massive Canchamaná Lateral Spread

During the earthquake, a massive liquefaction-induced lateral spread occurred in Holocene marine deposits in Canchamaná, 2 km north of Tambo de Mora, Peru. The GEER team documented this lateral spread in the field immediately after the earthquake, estimating it to be at least 3-km long by 1-km wide (Figure 1). At approximately the midpoint of this feature, the cumulative lateral displacement (obtained from adding up the widths of tension cracks) totaled more than 5 m (Meneses et al. 2009). However, due to its large size, it was difficult to quantify the magnitude and spatial distribution of the displacements in the field and to discern whether the entire feature moved as a coherent lateral spread toward the ocean. As detailed in Figure 1, the eastern boundary of the lateral spread was defined by the geologic interface between the marine deposits (with an approximate slope of 1.5-2.0%) and the Pleistocene Cañete Formation (a conglomerate with weak- to medium-cemented sandstone, siltstone, and claystone). The southern boundary of the lateral spread appeared to be defined by the interface of the marine deposits with Holocene alluvial deposits. The northern boundary was not firmly established in the field, as tension cracks and sand boils appeared to continue northward along the marine deposits, but time was not sufficient to allow for further exploration.

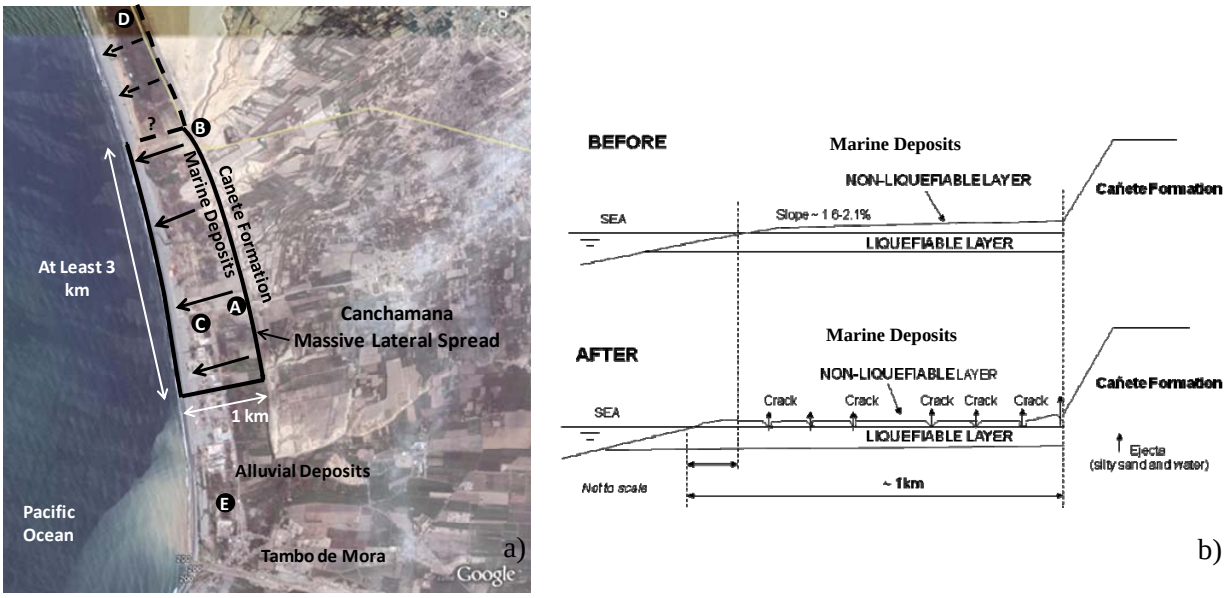

Figure 1. a) Approximate area of a massive lateral displacement in Holocene marine deposits at Canchamaná. The boundary of the mobilized area on the north is uncertain and could possibly extend further (background image from Google Earth); and b) Interpretative cross-sectional sketch of the massive lateral displacement.

A clear vertical offset (scarp) of variable magnitude was observed along much of the 3-km long geological interface between the marine deposits and the Cañete Formation. Along this scarp, a maximum vertical displacement of 3 m (Figure 2) was measured near Point A in Figure 1. In addition to the main scarp at the geological interface, numerous extensional ground cracks developed across the marine deposits parallel to the coastline. In general, the cracks were largest - both in terms of horizontal and vertical displacement - near the scarp and became smaller towards the coastline. Some crack widths were as large as 1 m and liquefaction ejecta were found inside many of them. At Point B, an approximately 8.0-m tall artificial fill embankment for the Pan American highway was severely damaged by liquefaction and lateral spreading of the marine deposits (Figure 3). Sand boils with diameters as large as 2 m were encountered near its base. Additionally, liquefaction and lateral spreading along the marine deposits contributed to collapse of the walls around Chincha Prison (Point C), resulting in the escape of more than 600 inmates. Just north of Point D (approximately 2 km north of Point B), a 400-m long, liquefaction-induced slope failure (Figure 4) damaged the Pan American Highway at Jahuay. This failure also occurred at the geologic interface between the Cañete formation and the marine deposits. However, due to the distance between these locations, it was not apparent if the Jahuay slope failure was actually a part of (i.e. initiated by) the Canchamaná lateral spread.

Satellite Image Processing

The Canchamaná lateral spread appears to be one of the largest lateral spreads (if not the largest) documented in historic times. However, due to the enormity of the feature and a limited time frame, it was difficult for the GEER team to firmly establish its boundaries in the field, spatially quantify the magnitude of the displacements, and discern if the entire area moved as a

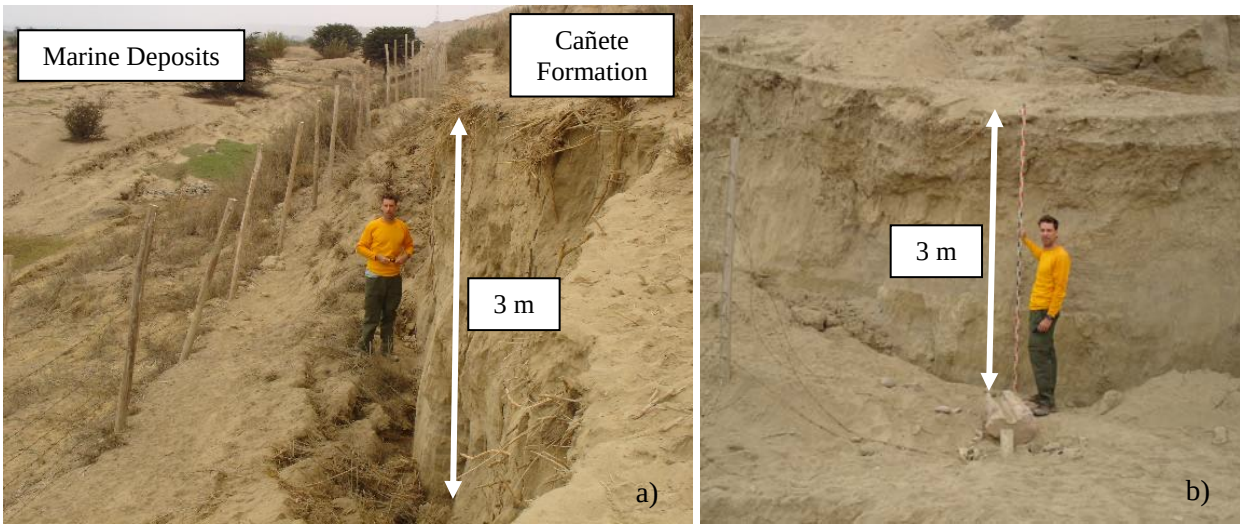

Figure 2. a) Maximum vertical offset of approximately 3 m (picture taken near Point A in Figure 1) along the scarp that developed at the interface between the marine deposits and Cañete Formation; and b) Same 3-m head scarp as viewed from the marine deposits looking toward the Cañete Formation.

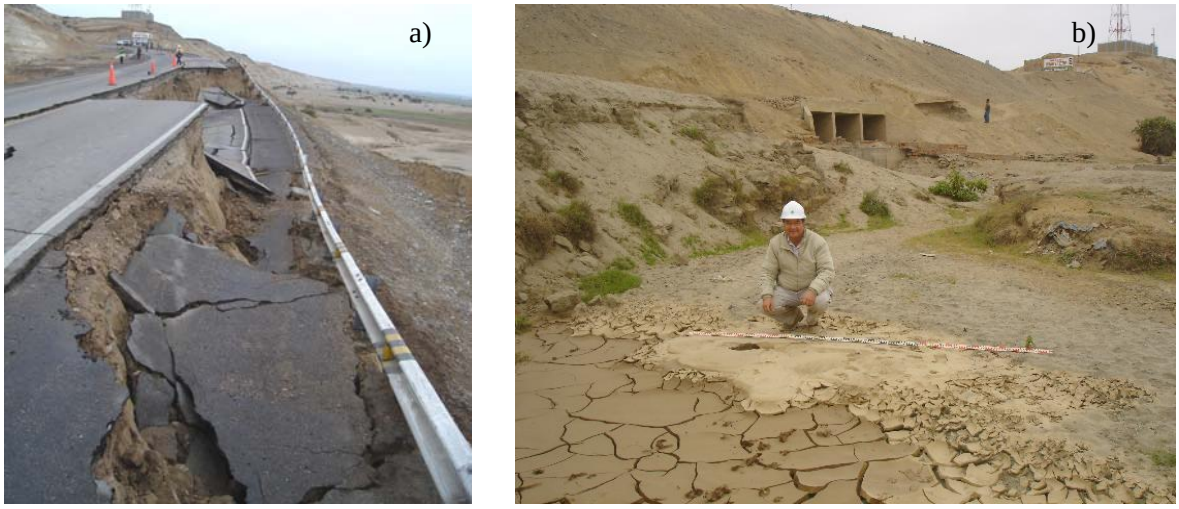

Figure 3. a) Liquefaction and lateral spreading of the marine deposits induced failure of the Pan American Highway embankment fill (picture taken near Point B in Figure 1) and sheared three concrete box culverts running through the embankment; and b) Sand boils as large as 2 m in diameter were found at the base of the embankment.

coherent lateral spread toward the ocean. Therefore, upon returning from Peru, pre-and post-earthquake high-resolution satellite images of the area were acquired by the GEER team and analyzed by personnel from the Center for Advanced Spatial Technologies (CAST, at the University of Arkansas) as a means to determine the magnitude and spatial variability of lateral displacements across the marine deposits. However, due to a limited budget of about $2,000, the satellite images could not be purchased as desired for optimum processing (both in terms of the raw data format and their areal extent).

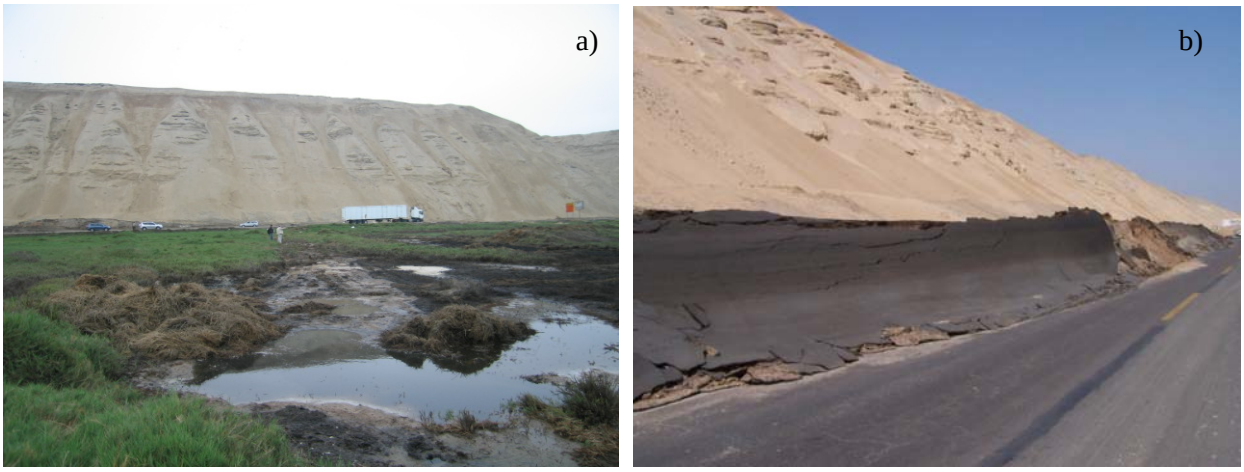

Figure 4. a) View of the Pan American Highway at the location of the 400-m long Jahuay slope failure (picture taken north of Point D in Figure 1). Marine deposits are in the foreground and the Cañete Formation in the background; and b) Pavement from the shoulder and north-bound lanes of the Pan American Highway were pushed into a near vertical face by the 400-m long failure.

A summary of the preliminary, limited-budget remote sensing analyses of the Canchamaná lateral spread (conducted by the authors in 2008-2009) is provided below, and is followed by a discussion of the proposed remote sensing plan that is a part of a recently funded NSF research project.

Preliminary Satellite Image Processing of the Canchamaná Lateral Spread

After the earthquake, pre- and post-event satellite images (Quickbird Ortho-ready Standard (ORS) product with 60 cm pixels) of the area were purchased by the GEER team and analyzed by personnel from CAST as a means to determine the magnitude and spatial variability of displacements associated with the lateral spread. The ORS product was not ideal for optimum processing, but was mandated by the constraints of a limited budget. Metadata delivered with the ORS images, describing the position and orientation of the satellite during acquisition, were used to model distortions caused by sensor orientation, while a digital elevation model (DEM) of the scene was used to remove relief induced displacements in the raw image. The DEM used in the preliminary analysis was a combination of Shuttle Radar Topography Mission (SRTM) – Level 1 DEM (90 meter resolution) and a 30 meter resolution DEM derived from the United States Geological Survey (USGS)-operated ASTER satellite (Welch et al. 1998). Twenty ground control points, collected to decimeter accuracy using carrier-wave differential GPS, were used in a least-squares adjustment to refine the satellite orientation parameters (Cothren 2005, Toutin 2004, Weser et al. 2008).

Results from preliminary analyses on these images (shown in Figure 6) confirm significant movement in the marine deposits relative to the Cañete formation, and indicate that the lateral spread may have extended at least another 3 km further to the north than originally documented in the field (resulting in a total feature length of approximately 6 km). Vector displacement estimates were based on a total of 223 ground features that were identifiable in

both the pre- and post-earthquake orthometric images (images free of distortions caused by sensor orientation and terrain relief). The lateral displacement of 92 measurement points on the marine deposits averaged 1.8 m, with a standard deviation of 1.0 m and a maximum displacement of 4.9 m. Twenty eight of these 92 points (30%) indicated more than 2 m of lateral displacement. The lateral displacement of the 131 non-marine deposit measurement points (including the Holocene alluvial deposits of Tambo de Mora) averaged 0.8 m, with a standard deviation of 0.5 m and a maximum displacement of 2.3 m. Only two of these 131 points (less than 2%) indicated more than 2 m of lateral displacement.

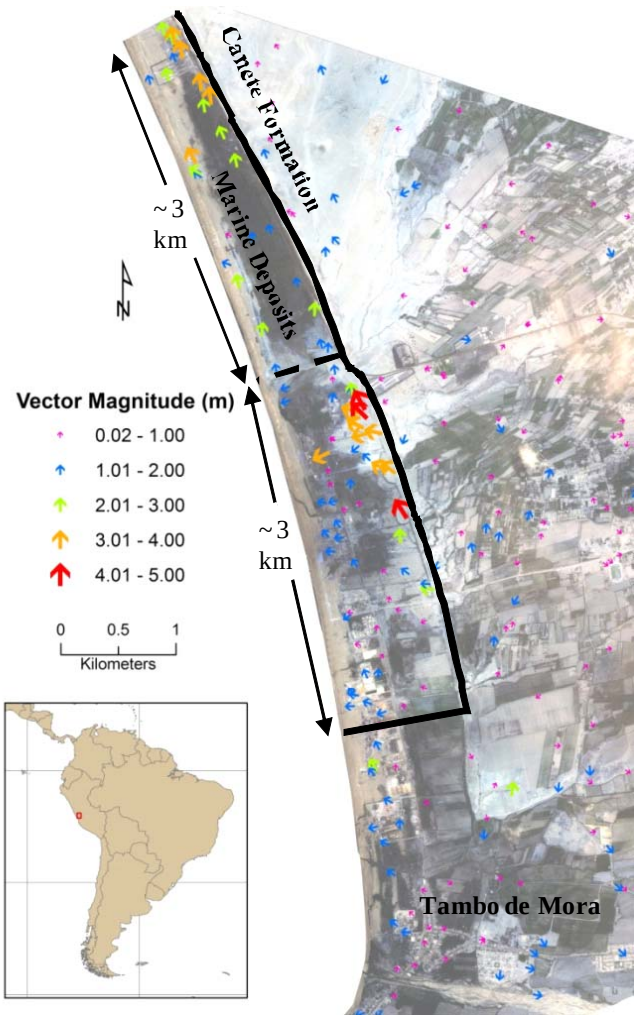

Figure 6. Displacement vectors obtained from preliminary satellite image processing of the Canchamaná lateral spread.

These results qualitatively confirm statistically significant relative movement between the marine deposits and the Cañete formation. However, the spatial variability of the displacement vectors likely do not support a block-type movement of the entire feature. Rather, as documented in the field, the largest displacements occurred in the marine deposits near the geologic boundary with the Cañete formation and generally tapered off towards the coast line. The following discussion explains why further, more detailed conclusions cannot be drawn from these preliminary results at the current time.

Preliminary Satellite Image Processing Concerns

Despite rigorous processing during the preliminary phase, there is reason to question the absolute validity of these results. Some of the vector displacements from the preliminary satellite image processing indicate movement in a direction contrary to what would be expected, and contrary to what was documented in the field. This discrepancy is most apparent for many of the vectors on the marine deposits furthest to the North, where movement is primarily indicated parallel to the coast rather than perpendicular to the coast. Three primary concerns that may have induced errors in the satellite image analyses are:

1. The Quickbird ORS product is intended for relatively low accuracy applications (although the pixel resolution of generated orthoimages is on the order of 0.6 m). The

Quickbird Product Guide predicts orthoimage accuracies (when generated using the process described above) in the range of 3-10 m when using a DTED Level 2 DEM and sub-meter GCP's. This is consistent with independent findings (Toutin 2004, Weser et al. 2008) and is due primarily to a simplified sensor orientation model. A complex model of this image formation process is available, but not provided with this lesser expensive product.

2. Relatively poor digital elevation data was available for the Canchamaná area. The SRTM Level 1 data that was available was not dense enough for the analysis that was attempted. Even when supplemented with the 30 m resolution ASTER DEM, it did not meet the DTED Level 2 tolerances generally expected from the USGS National Elevation Dataset (NED) in the continental U.S. Vertical inaccuracies in the combined DEM, caused by a variety of factors including vertical measurement error, horizontal displacement and low sampling rate, were on the order 7-15 m, and limited the horizontal accuracy of the orthophotos. Perhaps more important, the post-earthquake orthoimage was generated using a DEM that did not represent the actual terrain at the time of image acquisition.

3. While the GCP distribution was good, it was not optimal for the analysis. Most of the ground control was collected on the Cañete formation with a few points south of the marine deposits. The concentration of ground control on the higher elevation Cañete formation will bias the adjusted orientation, and thus bias the orthoimage at that elevation level and in that area.

While the preliminary lateral displacement measurements qualitatively indicate significant relative movement between the marine deposits and the Cañete formation and agree with field observations, they are also consistent with the error sources cited above. First, given the bundle adjustment results from the image processing, it is difficult to assign significance to the measured displacements in the marine deposits. One would expect to see sub-meter check point RMSE's to support a strong claim of significance. This was not achieved. Second, based on a coarse estimate of sensor orientation, a 10 m vertical error in the DEM would induce a 3 m horizontal shift to the south in the pre-earthquake image, but only a 0.5 m shift to the south in the post-earthquake image. When measuring relative movement, this would appear as a northerly displacement. This is consistent with the large northerly displacement measurements near the escarpment (nearly 5 m, Figure 6) where the DEM would be most inaccurate due to the low sampling rate. Furthermore, one would expect to see larger errors (which would appear as displacements caused by the event) on the marine deposits because of the concentration of ground control on the Cañete.

Proposed Satellite Image Processing of the Canchamaná Lateral Spread

The deficiencies of the preliminary analyses are currently being addressed as follows:

1. Pre- and post-earthquake Quickbird images with higher quality metadata are currently being obtained as part of a recently awarded NSF research project. The image product most suited for high accuracy photogrammetric analysis (including digital elevation model and orthophoto generation) is the Basic product. This more expensive image

product is delivered with the most rigorous and complex sensor orientation model available and has been shown to produce orthoimage accuracies in the 2-3 meter range when combined with DTED Level 2 elevation models (Noguchi et al. 2004) and even sub-meter accuracy when combined with better elevation models. No suitable Basic images acquired after the event exist in the archive, so the GeoEye-1 satellite has been tasked to acquire a stereo-pair (the GeoStereo product) of the Canchamaná area. The newly acquired images will provide much better orientation data which can be more rigorously refined in a GCP controlled bundle adjustment to achieve sub-meter check point RMS (Fraser and Ravanbakhsh 2009, GeoEye 2009). Furthermore, images with near vertical look angles will help to minimize orthoimage errors resulting from DEM errors.

2. The post-earthquake GeoEye-1 stereo-pairs will be used to generate a post-earthquake DEM of the marine deposits and the Cañete formation, which is more densely sampled and accurate than the DEM used in the preliminary analysis. The elevation model will represent post-event terrain at a 3-5 meter posting with vertical accuracies on the order of 2-3 meters (Fraser and Ravanbakhsh 2009, Liang et. al. 2007, Noguchi et. al. 2004). The new DEM, supported by sufficient ground control, will be used to produce much more accurate pre- and post earthquake orthoimages (expectations would be 1 m or better agreement with ground check points) and may even support a comprehensive analysis of extreme vertical displacements as a result of the event (Metternicht et. al. 2005, Tutsui et. al. 2007). In addition to the satellite derived DEM's, terrestrial LiDAR surveys will be obtained during the field campaign at selected locations along the escarpment. The sharp elevation changes in this area are difficult to model with even 0.5 meter resolution GeoEye-1 imagery, and the very high resolution terrestrial scan data can increase the accuracy of the post-event terrain model substantially.

3. During the field campaign, well distributed ground control will be collected with carrier-based differential GPS to complement the existing control. New points will be collected across the entire area and distributed in a way designed to yield the highest possible bundle adjustment accuracies of the GeoStereo images used for orthoimage generation (Fraser and Hanley 2005, Fraser and Ravanbakhsh 2009, Grodecki and Dial 2003, Holland et. al. 2007, Noguchi et. al. 2004). Redundant points will be collected and used as check points to better assess the accuracy of the resulting orthoimages and DEM. Furthermore, the GPS and terrestrial LiDAR work will be coordinated so that the high resolution point clouds and satellite derived DEM can more easily be combined.

Once this data has been collected and processed, the two orthoimages and associated DEMs can be used in a variety of ways to assess geomorphic changes. At a minimum, the following two mensuration tasks will be performed: First, the 223 identifiable points measured in the preliminary analysis will be re-measured on the new orthoimages to look again for horizontal displacements of the extended (6-km) stretch of the marine deposits relative to the Cañete formation. Second, the DEM and terrestrial laser scan data will be aligned using a combination of conjugant landmark measurements and the iterated closest point (ICP) technique to increase the accuracy, especially around the sharp geologic interface (Zhang and Cen 2007). The authors are confident that these analyses will allow the following questions can be answered: (1) What

was the areal extent of the lateral spread, (2) Did the marine deposits move as a coherent mass or did the failure consist of smaller blocks of independently moving soil, and (3) What was the magnitude of the lateral displacement and how did it vary spatially across the marine deposits? Once these spatial questions have been answered the following engineering questions can be investigated: (a) Why did the lateral spread occur over such a large area, (b) Why did the lateral spread stop where it did, and (c) What soil properties (type, stiffness, thickness, slope, etc.) influenced the magnitudes and directions of lateral displacement.

Conclusions

During the August 15, 2007 Pisco, Peru Earthquake (Mw=8.0), a massive liquefaction-induced lateral spread occurred in Holocene marine deposits near Canchamaná, Peru. However, due to the large size of the feature (at least 3-km long by 1-km wide), it was difficult to spatially quantify the magnitude of the displacements in the field, firmly establish its boundaries, and discern if the entire area moved as a coherent lateral spread toward the ocean. Preliminary satellite image processing has already qualitatively shown significant lateral movement of the marine deposits (up to 5 m). However, due to limitations in the initial satellite images and supporting data (ground truth, digital elevation models, etc.) the absolute magnitude and vector directions of the displacements obtained from the preliminary analyses are suspected not to be fully accurate. The future tasks of this research are to determine: (1) if high-resolution satellite image processing can be used to quantify the extent, magnitude, and direction of displacements associated with lateral spreading, and (2) what quality of raw satellite images and level of processing (i.e. cost) is needed to achieve accurate results.

Acknowledgments

Financial support for this research was provided in part by the U.S. National Science Foundation-sponsored Geo-Engineering Extreme Events Reconnaissance (GEER) Association through NSF Grant CMMI-00323914. Any opinions, findings, and conclusions or recommendations expressed in this material are those of the authors and do not necessarily reflect the views of the National Science Foundation.

References

Cothren, J., (2005). Reliability in Constrained Gauss-Markov Models: An Analytical and Differential Approach with Applications in Photogrammetry, *Report #473*, Geodetic and GeoInformation Science, Ohio State University, 61 pp.

Fraser, C.S., Hanley, H.B, (2005). Bias-Compensated RPCs for Sensor Orientation of High-Resolution Satellite Imagery, *Photogrammetric Engineering and Remote Sensing*, 71(8), 909-915.

Fraser, C.S., Ravanbakhsh, M., (2009). Georeferencing Accuracy of GeoEye-1 Imagery, *Photogrammetric Engineering and Remote Sensing*, 75(6), 634-638.

GeoEye, (2009). GeoEye-1 web site: *http://launch.geoeye.com/LaunchSite/about/Default.aspx* (accessed 21 October 2009).

Grodecki J., and Dial, G., (2003). Block adjustment of high-resolution satellite images described by rational polynomials, *Photogrammetric Engineering and Remote Sensing*, 69(1), 59-68.

Holland, D. A., and Mills J.P., (2007). ISPRS Workshop: High Resolution Earth Imaging for Geospatial Information, *Photogrammetric Record*, 22(119), 274-276.

INDECI (Instituto Nacional de Defensa Civil), (2007). http://www.indeci.gob.pe/ (accessed September 2007).

Liang-Chien, C., Tee-Ann, T., Jen-Yu W., and Jiann-Yeou R., (2007). Occlusion-Compensated True Orthorectification For High-Resolution Satellite Images, *Photogrammetric Record* 22 (117), 39-52.

Meneses, J.F., Franke, K.W., Cox, B.R., Rodriquez-Marek, A., and Wartman, J. (2009). Performance-Based Evaluation of a Massive Liquefaction-Induced Lateral Spread in a Subduction Zone, *IS-Tokyo 2009 - International Conference on Performance-Based Design in Earthquake Geotechnical Engineering - From Case History to Practice*, Tokyo, Japan, 15-17 June 2009.

Metternicht, G., Lorenz, H., and Radu G., (2005). Remote Sensing of Landslides: An analysis of the Potential Contribution to Geo-spatial Systems for Hazard Assessment in Mountainous Environments, *Remote Sensing of Environment* 98(2-3), 284-303.

Noguchi, M., Clive S. F., Takayuki N., Takahiro S., and Shoichi O., (2004). Accuracy Assessment of QuickBird Stereo Imagery, *Photogrammetric Record* 19(106), 128-137.

Rodriguez-Marek, A., Alva-Hurtado, J., Cox, B.R., Meneses, J., Moreno, V., Olcese, M., Sancio, R., Wartman, J. (2007). Preliminary Reconnaissance Report on the Geotechnical Engineering Aspects of the August 15, 2007 Pisco, Peru Earthquake: Report of the National Science Foundation-Sponsored Geo-Engineering Earthquake Reconnaissance (GEER) Team, Internet Report (http://gees.usc.edu/GEER/Peru_2007/Peru_2007_WebPage/index.html), Sept. 2007.

Toutin, T. (2004). DSM Generation and Evaluation from QuickBird Stereo Imagery with 3D Physical Modeling, *International Journal of Remote Sensing* 25(22), 5181-5192.

Tutsui, K., Rokugawa, S., Nakagawa, H., Miyazaki, S., Chin-Tung, C., Shiraishi, T., and Shiun-Der Y., (2007). Detection and Volume Estimation of Large-Scale Landslides Based on Elevation-Change Analysis Using DEMs Extracted From High-Resolution Satellite Stereo Imagery, *Geoscience and Remote Sensing, IEEE Transactions* 45(6), 1681-1696.

Welch, R., Jordan, T., Land, H., Murakami, H. (1998). ASTER as a Source for Topographic Data in the Late 1990s, *IEEE Transactions on Geoscience and Remote Sensing*, 36(4), 1282-1289.

Weser, T., Rottensteiner, F., Willneff, J., Poon, J., and Fraser, C.S., (2008). Development and Testing of a Generic Sensor Model for Pushbroom Satellite Imagery, *Photogrammetric Record*, 23(123), 255-274.

Zhang, T. and Cen, M., (2007). Robust DEM Co-registration Method for Terrain Changes Using Trimmed Squares Estimator, *Advances in Space Research*, 41(11), 1827-1835.